Spectrochimica Acta Part A: Molecular and Biomolecular Spectroscopy 305 (2024) 123496

Contents lists available at ScienceDirect

Spectrochimica Acta Part A:
Molecular and Biomolecular Spectroscopy

journal homepage: www.journals.elsevier.com/spectrochimica-acta-part-a-molecular-and-biomolecular-spectroscopy

Pushing measurements and interpretation of VCD spectra in the IR, NIR and visible ranges to the detectability and computational complexity limits

Marco Fusè [a], Giuseppe Mazzeo [a], Julien Bloino [b], Giovanna Longhi [a,c], Sergio Abbate [a,c,*]

[a] Dipartimento di Medicina Molecolare e Traslazionale, Università di Brescia, Viale Europa 11, 25123, Brescia, Italy
[b] Scuola Normale Superiore, Piazza dei Cavalieri, 56125, Pisa, Italy
[c] Istituto Nazionale di Ottica (INO), CNR, Research Unit of Brescia, c/o CSMT, VIA Branze 45, 25123, Brescia, Italy

GRAPHICAL ABSTRACT

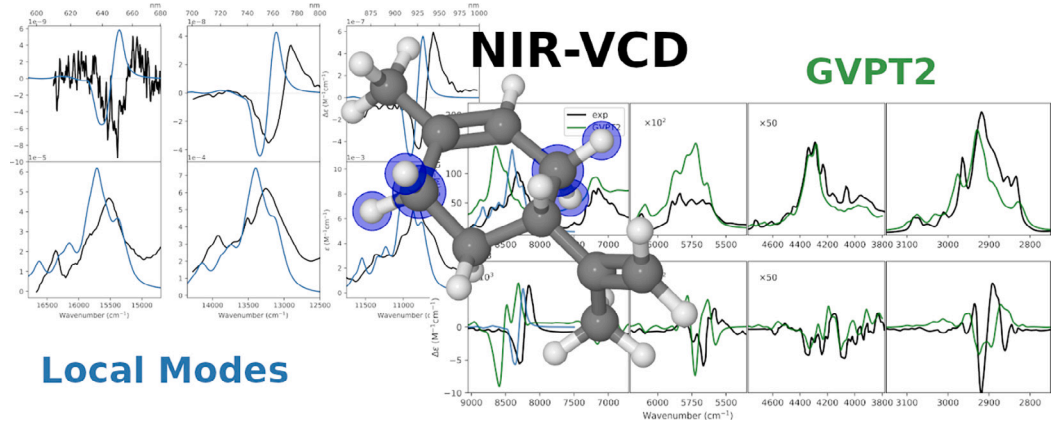

HIGHLIGHTS

- (*R*)- and (*S*)-Limonene VCD spectra measured in the range 900–16,000 cm^{-1}.
- GVPT2 calculations for the range 900–9000 cm^{-1} compare nicely to experiments.
- Local mode calculations for CH-stretching fundamental and overtones to 16,000 cm^{-1}.
- Local mode electrical anharmonicity up to 2nd order, Morse mechanical anharmonicity.
- VCD spectra in the NIR determined by 4 local modes over 13 total.

ARTICLE INFO

Keywords:
Vibrational Circular Dichroism (VCD)
Near Infrared (NIR)
Anharmonicity
Generalized Vibrational Perturbative Theory at the Second Order (GVPT2)
Local-mode approach
Limonene

ABSTRACT

(*R*)-Limonene VCD and IR absorption spectra for neat liquid samples are considered from 900 to 16,000 cm^{-1}, using mostly data by Nafie et al. up to 10,000 cm^{-1} and from previous investigations of the Brescia group. New VCD data are recorded in the merely overtone and combination region between 1800 and 2400 cm^{-1} and for the $\Delta n = 6$ overtone CH-stretching region above 15,000 cm^{-1}. The GVPT2 anharmonic DFT calculations permit satisfactory interpretation of the fundamental + overtone/combination of deformation modes in the mid-IR up to 3500 cm^{-1}. The GVPT2 approach is also used for the first CH-stretching overtone regions together with their combination with deformation modes up to 9000 cm^{-1}. Then the local-mode approach developed within the DFT protocol is employed in all the CH-stretching regions (fundamental + overtones) and is found to

* Corresponding author at: Dipartimento di Medicina Molecolare e Traslazionale, Università di Brescia, Viale Europa 11, 25123, Brescia, Italy.
E-mail address: sergio.abbate@unibs.it (S. Abbate).

https://doi.org/10.1016/j.saa.2023.123496
Received 5 July 2023; Received in revised form 29 August 2023; Accepted 4 October 2023
Available online 7 October 2023

satisfactorily account for the observed spectra, justifying the constant VCD pattern observed for all overtones. On the basis of the local-mode model the components of the bisignate VCD spectrum are attributed to the stretchings of the axial and equatorial CH bonds in α-position with respect to the ring CC double bond.

1. Introduction

Near Infrared (NIR) absorption spectroscopy covers the region from 4000 to 16,000 cm^{-1} (ca. 3300 to 625 nm) and is devoid of intense bands, since it contains the harmonically forbidden and thus very weak transitions associated with overtones and combinations [1,2]. Yet it is a fascinating region, being important, among the others, to explain the blue color of the sea as due to accumulated successive overtone absorptions, unique example of color originated from vibrational transitions [3]. The primary advantage of NIR spectroscopy, and the reason for its wide application (from biomedical diagnosis through agri-food to industrial QC/QA applications) stems from high permeability of most samples/materials against NIR wavelengths, with added advantage of non-destructive analysis and little or no sample preparation. [4–6]. Recently this spectroscopic region received renewed attention for investigating hydrogen bond properties [7–10] and, through it, for monitoring the earth atmosphere [11,12]. In this field we measured some time ago the vibrational circular dichroism (VCD) spectra corresponding to the weak NIR absorption between 1300 and 800 nm (7800–12,500 cm^{-1}) of limonene and two related compounds [13] plus some other compounds [14], coming second after the NIR-VCD measurement of Keiderling and Stephens [15]. The instrument we had used at the time was not tailored for that region and only strong NIR-VCD features could be detected. Subsequently we were able to set up a dedicated dispersive instrument, which permitted us to accurately investigate different sets of molecules [16] and to carry on, in parallel, a computational DFT analysis, mainly based on the local-mode approximation [17–19]. In these endeavors we were not left alone, since Professor Nafie and his group were able to set up an FT-NIR VCD instrument, measuring NIR-VCD spectra up to 10,000 cm^{-1} [20,21], which allowed us to cross-validate our results and to calibrate our measurements, both in frequency and intensity.

The local-mode approximation was quite acceptable, even in presence of relatively large numbers of oscillators and was recently confirmed by results obtained with full-*ab initio* GVPT2 DFT approach [8,22]. Yet, the first measurements on limonene, which, during earlier years, accumulated data up to 640 nm (15,600 cm^{-1}) [13,18,23] were never analyzed computationally, since the latter work was thought to be too demanding computationally.

In this work, we go back to the missing computational aspects of the first case, the measurement of which was made possible in the early days by the rather intense NIR-VCD signals. Indeed, the NIR-VCD bands of limonene have g ratios [24] of the order of 10^{-4} or slightly larger in most, if not in all, measured overtone regions [18], while, e.g., for methyl oxirane such ratio is closer to 10^{-5} [22], irrespective of the fact that methyl oxirane is rather rigid (excluding the methyls' hindered rotations) while limonene is more flexible and presents a number of independent conformers [25].

In Ref. [18], we reported the NIR-absorption and NIR-VCD spectra of (*R*)-limonene up to the 4th overtone ($\Delta n = 5$ quantum numbers in the CH-stretching vibrational modes). We repeated here the experiment for $\Delta n = 6$, which had been tried in Ref. [23], but with non-fully convincing outcomes. The VCD data were obtained as the semi-difference of VCD spectra of (*R*) and (*S*) enantiomers, after checking the signals of the two enantiomers being mirror images. Additionally, for the $\Delta n = 6$ case the VCD spectra of the racemic mixture was also considered, as explained in detail in the experimental part. The DFT calculations were conducted within the local-mode approximation, through an approach first presented in Ref. [17,26] and recently applied to methyl oxirane and methyl thiirane. We concentrate on the following aspects:

1. we first define how the four conformers previously found and described for limonene [25] contribute to the spectra. We then characterize the mechanical and electrical contributions to the anharmonicity for each one of the four conformers, each having 16 CH local-modes;
2. then we validate the local-mode approach by comparing it with the results obtained for lower Δn on the basis of the GVPT2 approach, recently updated from previous investigations of anharmonic molecular aspects [22,27,28].
3. we investigate the relative importance of electrical and mechanical anharmonicity in explaining the observed data;
4. among all the computed transitions, we will extract the local-modes mostly responsible for the observed VCD signals;

2. Experimental and theoretical/computational methods

2.1. Spectroscopic measurements

While the VCD data for the fundamental and first four overtone transitions of the CH stretching vibrations of (*R*)-limonene were taken from Refs. [20,29], on neat liquid samples, the experimental VCD spectra of both limonene enantiomers and of the racemic mixture thereby in the 680–620 nm range were recorded for this work with a Jasco J-815SE spectrometer, with an added special sample compartment. Data were taken with neat samples contained in an home-built quartz cell of 19 cm in pathlength. The scanning speed was 10 nm/min and resolution was set to 10 nm. One hundred data accumulations were recorded for each sample and their result is reported in Figure S1. In the main text of the work we report the semi-difference of (*R*) and (*S*) data. Data were also collected in the 800–700 nm range producing spectra in good agreement with those already reported in literature [23,29].

The experimental absorption spectrum of limonene in the 680–620 nm range were recorded with a Jasco V-520 spectrometer, data were taken with neat liquid samples contained in a quartz cell of 10 cm in pathlength averaging over 20 accumulations.

For the region 1700–2400 cm^{-1}, VCD measurements were carried out with a Jasco FVS6000 instrument, which is a FTIR instrument with added linear polarizer and ZnSe photo-elastic modulator to achieve VCD measurements. A liquid N_2-cooled HgCdTe (MCT) detector was employed (resolution 4 cm^{-1}). Neat liquid samples were contained in BaF_2 500 μm pathlength cell and 6000 scans were accumulated for each spectrum and the reported data are averages over the accumulated spectra.

2.2. Computational details

Unless specified otherwise, calculations were performed with the Gaussian16 suite of quantum chemical programs [30]. Based on the extensive benchmark analysis from ref [27], the combination of the B3PW91 [31] functional and the jun-cc-pVTZ [32] basis set was used, hereafter labeled PW91. We did not use empirical dispersion (D3BJ) corrections in geometry optimization since they lead to relative abundances not in agreement with the experimental data previously reported in literature [25,33,34].

Geometry optimizations were performed with tight convergence criteria (i.e. 1×10^{-5} hartree/bohr and 4×10^{-5} bohr on RMS forces and displacements, respectively, with thresholds for the maximum values being 1.5 times larger), and minima were confirmed by Hessian evaluations. Harmonic energies and intensities were obtained using analytic second derivatives of the energy and first derivatives of the properties of interest, whereas higher-order derivatives were computed

through numerical differentiations using a step of 0.01 $\sqrt{\text{amu}}$ Å for the displacements along the mass-weighted normal coordinates.

Since all the experimental spectra were recorded for neat liquid, in absence of a reliable implicit solvent model, we opted to employ gas-phase calculations in all the investigated regions, as already done in similar conditions [22].

2.3. GVPT2 calculations

Anharmonic calculations, up to three quanta transitions [35], were performed with the GVPT2 model as implemented in a development version of the Gaussian suite of programs [36]. In the GVPT2 framework, the diverging terms are removed from the perturbative expressions (therefore leading to the so-called IDVPT2 [27] level), and then reintroduced through a variational step on the reduced-dimensionality set. Resonances are identified through an automatic procedure, which accounts for both energy and intensity as described in Ref [37]. The procedure relies on two sets of tests to identify automatically Fermi and 1–1 or 1–3 Darling–Dennison resonances, one rooted into the definition of the energies and one designed to account for the specificities of the intensities. For Fermi resonances, the standard Martin test [38] is complemented by a new one based on the coefficients of the perturbed expansion of the wave function. For 1–1 and 1–3 DDRs, the existing test based on the magnitude of the Darling–Dennison term for the energy is also supplemented by a similar test that relies on the magnitude of the relevant coefficients of the perturbed wave function. More details on the definition as well as suitable values for the thresholds can be found in Ref. [37]. The criteria used in the identification of Fermi and Darling–Dennison resonances through two-step procedures are summarized below:

1 – 2 Fermi resonances: Maximum frequency difference 200.0 cm^{-1}; Minimum difference PT2 vs variational 1.0 cm^{-1}; Intensity-specific term 1.0 (as defined in Ref. [27]); 2 – 2 Darling–Dennison resonances: Maximum frequency difference 100.0 cm^{-1}; Minimum value of off-diagonal term 1.0 cm^{-1}; 1 – 1 Darling–Dennison resonances: Maximum frequency difference 100.0 cm^{-1}; Minimum value of off-diagonal term 10.0 cm^{-1}; Intensity-specific term 1.0; 1 – 3 Darling–Dennison resonances: Maximum Frequency difference 100.0 cm^{-1}; Minimum value of off-diagonal term 1 cm^{-1}; Intensity-specific term 0.025.

Calculation analysis and the plotting of the simulated spectra were supported by the estampes [39] Python library for data processing and matplotlib graphical library [40].

2.4. Local-mode model

As described in the work [22] and following closely the notation introduced by Paoloni et al. [8], we numerically defined the first and second derivative with respect to the CH-bond length of the Atomic Polar Tensors (ATP, Π) and the second derivative of the Atomic Axial Tensors (AAT, A) of C and H for all CH bonds. Having taken into account electrical anharmonicity up to the third order in this way, we dealt with mechanical anharmonicity in the following way: first the transition energies from the ground to the excited states of one of the 16 CH stretching vibrations ($l = 1, 16$, related to the two groups CH_3, to the three CH_2 groups, to the C*H and to the three olefinic =CH bonds) have been assumed to have the form [41,42]:

$$\epsilon_{0\to n_l} = hc\left[n_l\omega_{0,l} - \chi_{ll}n_l\left(n_l+1\right)\right] \tag{1}$$

with n_l the number of quanta is associated to the CH bond l, and the parameters ω_0 and χ (in wavenumber units) determined by the Morse potential parameters D and α namely (omitting from now on the bond label l):

$$\omega_0 = \frac{1}{2\pi c}\sqrt{\frac{2D\alpha^2}{m_R}} \qquad \chi = \frac{\alpha^2\hbar}{4\pi c m_R} \tag{2}$$

m_R being the reduced mass of the CH bond, ca. (12/13) amu, and the other constants besides the Morse potential dissociation energy parameter D ($D = \frac{\omega_0^2}{4\chi}$, in cm^{-1}) and the α parameter describing the approach to dissociation as dictated by the ratio $\frac{\omega_0}{\chi}$, being obvious fundamental constants. Second, the infrared intensities and the VCD rotational strengths were calculated with the following equations:

$$\langle 0|\mu_j|n\rangle = \sum_{\alpha=H,C}\Pi_{\alpha,jz}(0)t_\alpha\langle 0|z|n\rangle + \frac{1}{2}\sum_{\alpha=H,C}\left(\frac{\partial\Pi_{\alpha,jz}}{\partial z}\right)_0 t_\alpha\langle 0|z^2|n\rangle + \frac{1}{6}\sum_{\alpha=H,C}\left(\frac{\partial^2\Pi_{\alpha,jz}}{\partial z^2}\right)_0 t_\alpha\langle 0|z^3|n\rangle \tag{3}$$

$$\langle 0|m_j|n\rangle = \sum_{\alpha=H,C}A_{\alpha,jz}(0)\frac{1}{m_R}t_\alpha\langle 0|p|n\rangle + \sum_{\alpha=H,C}\left(\frac{\partial A_{\alpha,jz}}{\partial z}\right)_0\frac{1}{m_R}t_\alpha\langle 0|zp|n\rangle + \frac{1}{2}\sum_{\alpha=H,C}\left(\frac{\partial^2 A_{\alpha,jz}}{\partial z^2}\right)_0\frac{1}{m_R}t_\alpha\langle 0|z^2p|n\rangle \tag{4}$$

Π_α and A_α being APT and AAT tensors (α being the atoms C and H involved in the CH-stretching under consideration), together with their obvious first and second derivatives.

z is the displacement coordinate along the CH bond, along which the z-axis is oriented, j stands for generic Cartesian component ($j = x, y, z$) and t_α(α = C or H) represents the local eigenvector as defined in Ref. [8]. The transition integrals, up to $n = 6$, appearing in Eq. (3) and (4) are given in Tables S2–S4 of section S4 in the Supplementary Information file (SI) together with some consideration about their derivation and calculation that may be useful accounting for MVCD spectra [43].

A useful parameter introduced to deal with these transition moments is the length parameter d defined by:

$$d^2 = \frac{\langle 0|z^2|0\rangle}{4\pi^2} = \frac{\hbar}{2cm_R\omega_0} \tag{5}$$

which is thus proportional to the average harmonic displacement in the ground state.

Local mode calculations were performed with an in-house developed set of python scripts which prepares and processes Gaussian files and is freely available for any interested reader [44].

3. Results and discussion

As already reported, the most stable conformers show a half-chair conformation of the six-membered ring with the isopropenyl group in equatorial position (Fig. 1). The latter is true for the next two conformers, while the first conformer with the axial isopropenyl group comes fourth with just 4% of the total population. The first three conformers are the obvious rotational isomers, where the isopropenyl group differs by a rotation of about ≈120° around the CC bond. Interestingly, we noticed that the use of the widely employed D3BJ dispersion causes an overestimation of the population for one of the axial conformation. The conformers reported in Fig. 1 are quite close to those first introduced by Aviles Moreno et al. [25], with quite similar population ratios as well.

Following the work plan presented in the Introduction section, we next calculated the IR and VCD spectra with the GVPT2 approach. Results are reported in Fig. 2 and are compared with the experimental spectra recorded for neat liquid samples. For the latter we relied on the results by Nafie et al. [20], except, in the top panels, where we report our own data, for the mere overtone/combination range 1700–2400 cm^{-1}. Results in the mid-IR range (Fig. 2, top two rows) are excellent, except for the 1700 and 1450 cm^{-1} absorption features whose transition energies are overestimated: this inconsistency appears for the C=C stretching and HC=C bending 1-quantum normal modes and is already observed at the harmonic level suggesting a poor description of this type of modes. On the other hand, the anharmonic

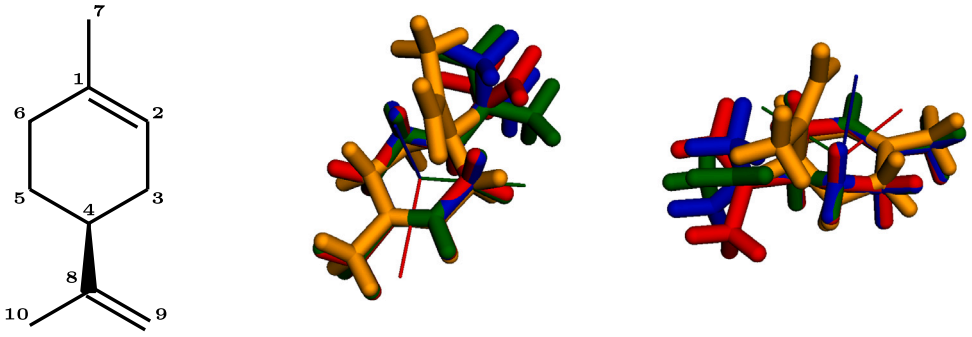

Fig. 1. Graphical representations of the superposed structures of the four most stable conformers of limonene.

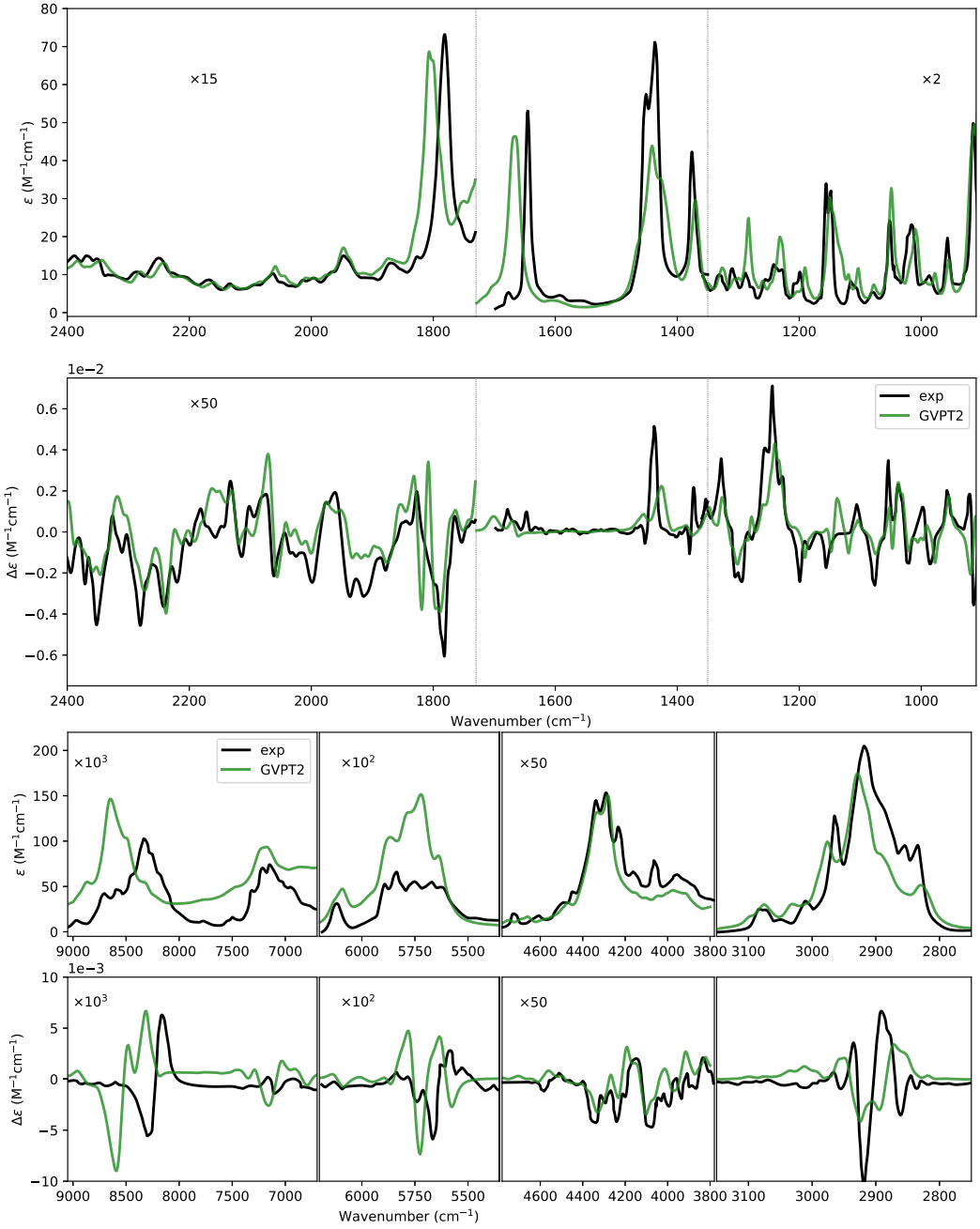

Fig. 2. Comparison of the experimental IR and VCD spectra (black lines) of (*R*)-limonene with anharmonic calculations in the 950–9000 cm^{-1} range (colored lines). Calculations were performed at the PW91 level. The spectra were simulated assigning Lorentzian distribution functions with: 4, 10, 20, 30 cm^{-1} half-width at half-maximum from small to high wavenumbers. With the exception of the 1700–2400 cm^{-1} range measured in this work, the VCD and absorption experimental spectra are taken from Ref. [20].

treatment corrects well the overestimation of the absorption intensity computed at the harmonic level. We would like to point out that the mere overtone/combination range 1700–2400 cm^{-1} is excellently predicted, both in IR and in VCD, with rare discrepancies; this goes along with our previous investigation of this very same region for the rigid three-membered ring compounds methyl thiirane and methyl oxirane. The next regions deal with CH stretching in the range from 2750 to 9000 cm^{-1} and are reported in the lowest two rows of panels. From right to left, the calculated fundamental CH-stretching region shows some discrepancies with the experiment whereas the 1-quantum/CH stretching+1-quantum/deformation combination region is excellently predicted by GVPT2 calculations. Moving to the 2-quanta/CH stretching region, the IR intensities are overestimated for the CH-aliphatic stretchings and the NIR-VCD data are not well predicted, possibly for the overestimate of the calculated frequencies. Finally, we have the 2-quanta/CH stretching overtones in combination with 1-quantum deformation modes on the right and the 3-quanta/CH stretching overtones on the left part of the last panel. In this case, the overall IR and VCD intensities are correctly evaluated, but the frequencies are overestimated. The latter fact might be related to the mismatch in the precedent region and is also observed in the ensuing overtone regions, also in the local-mode approximation (*vide infra*). In any case, with the exception of the CH-stretching fundamental region, we can say that the overall prediction of the fundamental and low overtones/combinations regions from mid to near-IR range, is very good, also taking into account that at least three conformers participate substantially in the limonene population.

As the third step of this investigation, let us take a look at the prediction of fundamental to $\Delta n = 6$ overtones for the CH-stretching modes in the local-mode approximation. Results are given in Fig. 3: the fundamental $\Delta n = 1$ region is well predicted by the local-mode approach in absorption, while in VCD the intensities are underestimated, but the sign progression of bands is correctly predicted. In the first overtone $\Delta n = 2$ region the IR spectrum is overestimated in intensity with respect to experiment, and also its form is not well accounted for. This result is in some way similar to the ones obtained with the perturbative approaches based on the normal-mode representation. In Figure S2 in SI the IDVPT2 spectra were added to the GVPT2 ones in order to evaluate the impact of the variational corrections and to allows an easier connection with the normal modes along which the properties derivatives were calculated. The VCD spectrum, instead, is accounted for by the local-mode calculations in sign and intensity, except that experiments by the group of Nafie present several resolved features within the bisignated group, which the local-mode approximation seems not capable of predicting. In the next overtone regions, namely $\Delta n = 3$, $\Delta n = 4$, $\Delta n = 5$ and $\Delta n = 6$ the local-mode approximation performs well regarding the overall intensity (for NIR absorption and NIR-VCD) and in sign (for NIR-VCD). One slightly critical result is worth pointing out, though, namely the mismatching of the band positions, which progressively worsen with the increasing quantum numbers and is particularly evidenced by the error on the central peak in the NIR absorption spectra and by the frequency offset in the two components of the bisignate NIR-VCD spectra. The latter aspect might be related to an underestimation of the χ parameters or to an overestimation of ω_0. Overall, though, the calculated spectra from $\Delta n = 3$ to $\Delta n = 6$ are quite acceptable and allow us to evidence two main virtues of the present calculation. The assumption made on the electrical and mechanical anharmonicity terms discussed above appears to work: namely the third order terms for electrical anharmonicity seem accurate enough to reproduce intensities and the Morse type anharmonic potential is appropriate. Furthermore, we point out that the assumed bandwidth, which is progressively increasing from $\Delta n = 1$ (10 cm^{-1}) to $\Delta n = 2$ (20 cm^{-1}) to $\Delta n = 3$ (30 cm^{-1}) to $\Delta n = 4$ (60 cm^{-1}) and 100 cm^{-1} for $\Delta n = 5,6$ appears quite tenable, and is comparable to what had been observed by Reddy, Heller and Berry on $\Delta n = 5$ to 6 and 7 for the overtone spectra of benzene [45].

As the fourth and final step, we come to analyze the most important modes explaining the main features of the IR and VCD spectra in Fig. 3, especially in relation to the constant behavior of the NIR-VCD bisignate spectra. A first observation is that, except for the least populated conformer, all conformers show the same intense bisignate feature from the first up to the fifth overtone (see Figure S3), which is therefore connected to the half-chair configuration of the ring. Indeed, the conformer with the opposite half-chair configuration still presents a strong bisignate signature but with opposite signs. As highlighted in Figures S4/S5 and S6/S7, and in agreement with the experimental data, such features are associated with the least energetic local-mode transitions related to pseudo-axial and pseudo-equatorial CH_2 on the ring, which turn out to be those in α position with respect to the double bond in the ring (marked as C_3 and C_6 in Fig. 1).

Such scheme is not working in the fundamental region, where, for instance, the most intense negative VCD peak at about 2930 cm^{-1} is associated with the CH_2C^*H stretching in both the local- and the normal-mode representations (see also the first interpretation of the fundamental region, based on a normal mode scheme [46]), whose contribution begins to be non-negligible again from the fourth overtone (see Figure S7). We think that the origin of the simplification of the signal should be sought in the so-called *electrical* anharmonicity or more generally in the contributions to anharmonicity from higher-order derivatives of the properties, which increases in relevance moving from the fundamental to the overtones. Hence it is instructive to consider the atomic polar tensors Π and the atomic axial tensors A and their derivatives with respect to CH-bond elongations (see Figure S8 for an example of representation of the CH frame), obtained by polynomial fit and reported in Figure S9 for the most populated conformer. As expected, the main component of Π lies along the stretching direction z, even though smaller but non-negligible components are present also in the other two directions. For A the major components are perpendicular to z. Focusing our attention on the ring's CHs and in particular on the CHs in the α positions with respect to the double bond, one may appreciate that the major components lie on the axis directed toward the double bond (x axis in Figure S8), with opposite signs for axial and equatorial CH at the equilibrium. Smaller components are observed along the displacement axis z, where, however, the clear separation in sign behavior between the different CH orientations is not kept for all the CH_2. The alternation of signs instead is apparent in the first derivative of $\partial A_z/\partial z$ (see Figure S10). In Figures S11 and S12 representations of the Taylor-series term contributions of Eqs. (3) and (4) to the overall VCD signals of the two C_6H and a 3D representation of the total $\boldsymbol{\mu}$ and $\boldsymbol{m}$ dipole transition moments and the contributions of each term are reported respectively. In fact, starting from the first overtone, the relative weight of the terms with the first derivatives of Π and A substantially increases, leading to the characteristic bisignate shape observed in the VCD spectra.

On the other hand, a clear prevalence of few transitions is not observed in the absorption spectra, where the inclusion of all CH stretchings is required to reproduce the experimental spectra. The latter finding is in line with the basic local-mode model originally proposed by Henry [47], for which the total absorption is proportional to the number of local-modes. As expected, contributions arising from the second derivatives of Π and A have some relevance starting from the fourth overtone (see Figures S13 and S14), which is one of the reasons why at higher number of quanta VTP2 is not applicable and higher-order (VPT4, VPT6) would be required.

From the results presented in the SI (Figures S4/S5 and S6/S7), it is clear that the two VCD components are due to the pseudo-axial and pseudo-equatorial CH-bond stretchings located at positions 3 and 6 (see Fig. 1). The former appears at lower frequencies and is characterized by a positive VCD, while the latter, at higher frequencies, shows a negative VCD for (*R*)-limonene. The other modes make negligible contribution to the VCD signal, while all CH-stretchings contribute to the same extent to absorption. While the difference in frequency of

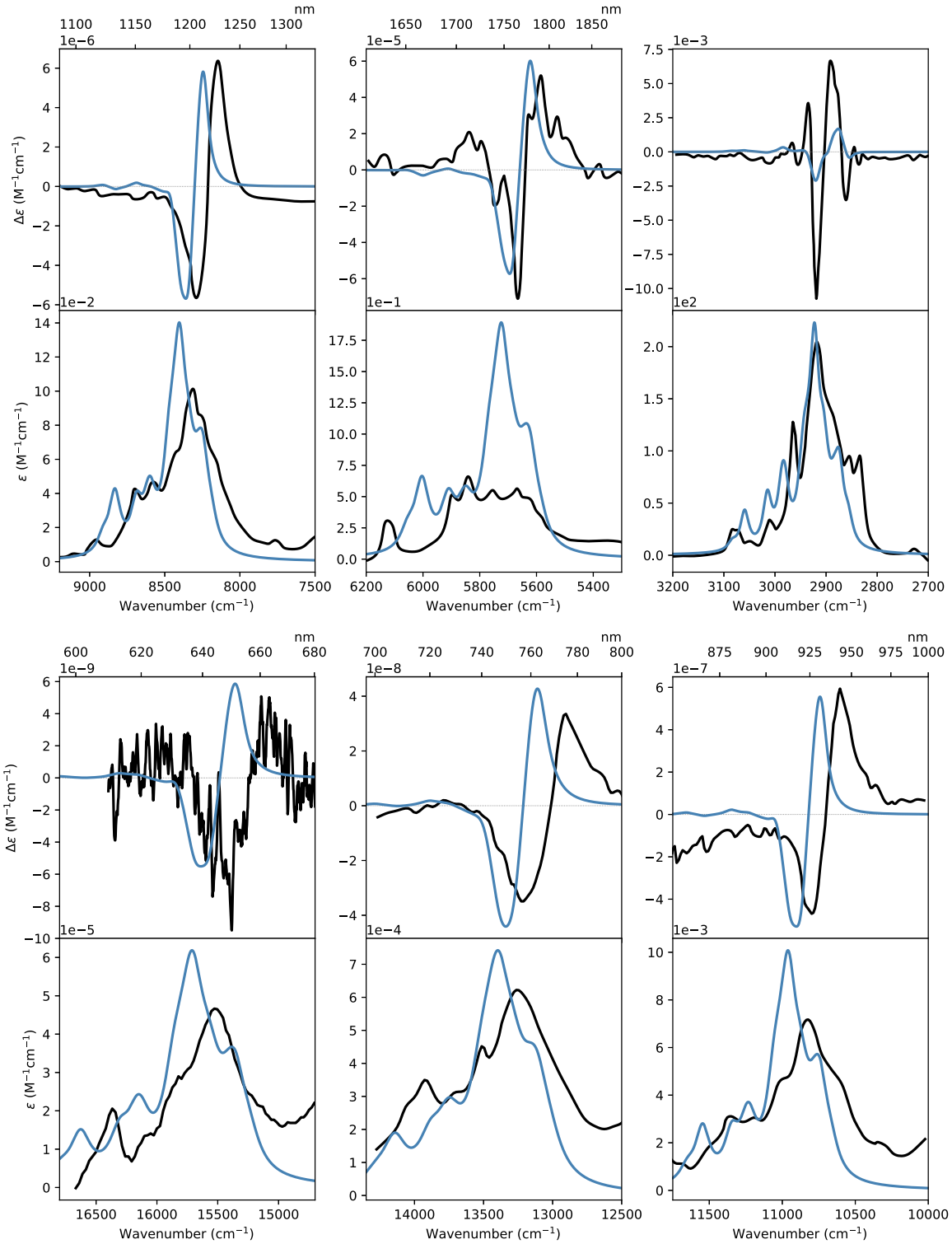

Fig. 3. Comparison of the experimental IR and VCD spectra (black lines) of (*R*)-limonene with local-mode calculations range (colored lines) of fundamental CH-stretching region and its overtones up to the fifth. Calculations were performed at the PW91 level. The spectra were simulated assigning Lorentzian distribution functions with: 10, 20, 30, 60, 100 and 100 cm^{-1} half-width at half-maximum from small to high wavenumbers. The VCD and absorption spectra reported up to $\Delta n = 3$ are taken from Ref. [20], $\Delta n = 4$ and $\Delta n = 5$ are taken from Ref. [29] and $\Delta n = 6$ data were recorded in this work.

axial versus equatorial has been documented in many different ring molecules, as originally proposed by McKean [48], Longhi et al. [49,50] and Paoloni et al. [8], the peculiar intensity behavior of the CH-stretchings in positions 3 and 6 is explained by their proximity to the double bond of the ring.

In order to investigate the role played by the double bond in α position, we performed local-mode calculations at different torsion angle on the minimal template system depicted in Fig. 4 representing the C_5–C_6–C_1=C_2 fragment of the original molecule. The model system was built by extracting the four carbon atoms from the structure of the

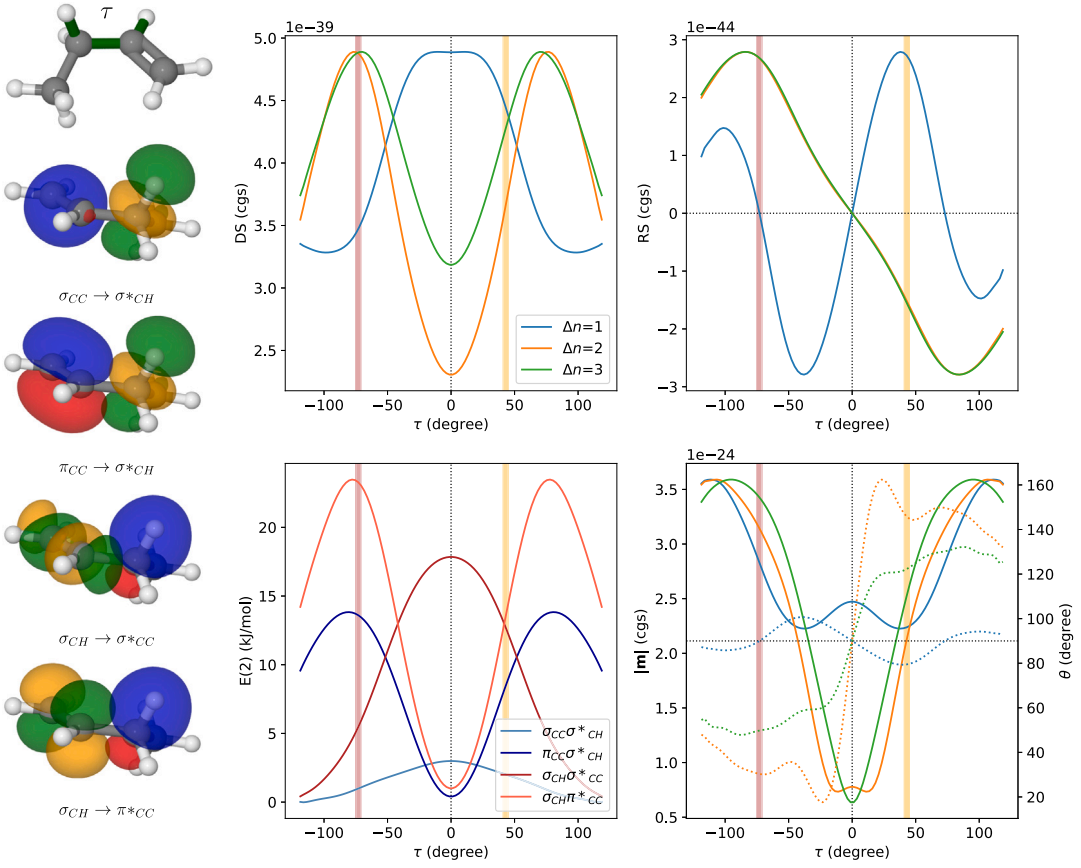

Fig. 4. Upper panels: dependence of the dipole strength (DS) and the rotatory strength (RS) of CH stretchings related to the CH_2 group computed in local-mode on the dihedral angle τ (depicted as green bonds in the top left of the figure). Values of DS and RS for Δn = 2,3 were normalized with respect to the fundamental ones (normalizing factors DS: 65, 941; RS: 8, 105). Lower panels: on the left, representation of the NBO stabilization energy E(2) [51–53]; on the right, magnitude of the magnetic dipole transition moments ($|\mathbf{m}|$, normalizing factors 49, 400) and angle θ between $\boldsymbol{\mu}$ and $\mathbf{m}$ as function of τ (dashed lines). The involved NBO orbitals are depicted in the left part of the figure, occupied orbitals in red/blue and unoccupied ones in green/orange. The dihedral values assumed by the equivalent CH bonds in limonene indicated with red (pseudo-axial) and orange (pseudo-equatorial) vertical bars in all graphics.

most populated conformer and saturating the valence with hydrogen. Then, a relaxed scan along the τ dihedral angle (stepsize = 2.5°) was performed and local-mode calculations were done at each step for the CH_2 bonds.

In the top part of Fig. 4, we report the dependence of dipole and rotational strengths on the dihedral angle defined by one aliphatic CH bond and by the methine CH bond of the vinyl group. Since in limonene the fragment is inserted in an unsaturated six-membered ring, at the equilibrium geometries the values of τ are locked by the half-chair configuration of the ring to $\tau \approx -72°$ and $\tau \approx 42°$ depicted as red and orange vertical lines respectively in the figure. Despite its extreme simplification, the model is capable of representing the system as can be seen by comparing calculated values of the dipole strength (DS) and of the rotatory strength (RS) for the template with those in Table S5. As already described for the whole system, the major differences are observed between fundamental and overtones, with the latter behaving uniformly, in particular for VCD (all Δn = 2–6 curves for RS versus τ are superimposable, once normalized). The shapes of the curves suggested us a connection to the different molecular orbitals involved. Indeed, inspired by the works of Nafie and coworkers on localized molecular orbital [54,55] and by the recent works of Yabushita et al. on overtone absorption intensities studied by examining the electron density derivatives [56,57], we built a qualitative picture of the interaction of the molecular orbitals localized on the CH and CC bonds. To this end, we performed an NBO analysis [51–53] of the system along the scanned dihedral angle and plotted the stabilization energies E(2) between the set of occupied and unoccupied orbitals. The results are reported at the bottom of Fig. 4 and the orbital representations are given on the left side of the same figure.

The NBO representation evidences a noteworthy correlation between stabilization energy and dipole strength values. Indeed, the σCH-σ*CC energy term exhibits the same trend as DS for the fundamental transition, while interactions σCH-π*CC and πCC-σ*CH show a minimum when the CH is in the nodal plane of πCC, as expected. In the latter case, the trend correlates with the calculated DS of the overtones. Considering RS, the interpretation is less immediate, it is nearly zero for the fundamental transition for the pseudo-axial CH (CH_{pax}) and positive for the pseudo-equatorial CH (CH_{peq}). Instead, the RS of all overtones coincide (after normalization) and are positive for CH_{pax} and negative for CH_{peq}. In order to disentangle the different contributions to the RS values, it is useful to report the magnitude of $\boldsymbol{m}$ and the values of the angle θ between $\boldsymbol{\mu}$ and $\mathbf{m}$ as function of τ, in the bottom right panel of Fig. 4. In this way, a correlation between the NBO delocalization energies (E(2)) and $|\boldsymbol{m}|$ becomes apparent. However, contrary to what was observed for DS, π-type interactions seem to contribute to $|\boldsymbol{m}|$ already for the fundamental (Δn = 1) transition. The Δn = 1 trend for $|\boldsymbol{m}|$ recalls the shape of a curve obtainable by summing the π-type and σ-type E(2) plots. For values of τ close to zero, $|\boldsymbol{m}|$ can be related to σ-type interactions, while for τ angles approaching 90° the π-type interactions are expected to prevail. Also, the analysis of θ versus τ shows a qualitatively different behavior between fundamental and overtones that can be related to the importance of both σ and π-type interactions for fundamentals while π-type ones play a major role for overtones. In fact, we may notice that at high $|\tau|$ values, with τ smaller than −70° or larger than 70°, θ is smaller/larger than 90°

respectively for both fundamentals and overtones since in this region π-type interactions dominate. On the contrary at small values of τ, the σ-type interaction dominates and causes a change in the relative orientations of $\boldsymbol{\mu}$ and $\boldsymbol{m}$, eliciting a change of sign for the RS of the fundamental compared to overtones. In conclusion, for the examined overtone transitions (Δn = 2–6), the RS sign of the CH stretching depends mainly on its relative position, above or below the nodal plane of the C=C double bond and consequently depends on their π-type interactions. We may conclude that the RS of the locked α-CH_2 in the limonene structure explains the strong and coherent bisignated VCD signal observed in all the experimental overtone spectra of limonene.

4. Conclusions

In this work, we have investigated the full IR absorption and VCD spectrum of neat (*R*)-limonene, from 900 to 16,000 cm^{-1}. GVPT2 anharmonic DFT calculations permit satisfactory and in certain regions excellent interpretation in the range 900–10,000 cm^{-1}, with few exceptions, the most critical among the latter being the fundamental CH-stretching region from 2800 to 3500 cm^{-1} and the first overtone between 5000 and 6500 cm^{-1}. In general, the method works quite well in the mid-IR range and typical combination regions (1:1 stretching–bending combinations 3600–4600cm^{-1} and 2:1 stretching-bending combinations 6500–7500 cm^{-1}) not represented at all by the local-mode model. The local-mode approach developed within the DFT protocol is employed for all the CH-stretchings regions (fundamental + overtones) and is found to satisfactorily account for the observed spectra, except for the first overtone region between 5000 and 6500 cm^{-1}, where both the methods here tested fail. The latter discrepancy was expected, since that region in the case of CH stretching is neither in the normal nor in the local-mode regime [58]. From the second to the fifth overtone, VCD spectra were observed and were adequately explained in terms of the two pseudo-axial and two pseudo-equatorial CH stretching local-modes in α-positions with respect to the ring double bond. That is to say, the two components of the bisignate VCD spectrum observed for all overtones from Δn = 3 to Δn = 6 are attributed to the stretchings of the axial and equatorial CH bonds in α-position with respect to the ring CC double bond, which provides intensification of the rotational strengths of four modes over the other 9 local-modes, while the dipole strengths are similar for all 13 local-modes. In the Results and Discussion section we provided arguments based on molecular orbital interaction which allows one to understand why the local-modes of these four CH stretchings have the observed VCD signs and intensities. The normal mode interpretation of the fundamental CH-stretching region is quite different and is based on the $CH_2CH_2C^*H$ inherently dissymmetric chromophore [46]. As a final note, we point out that the realm of overtones and combinations in chiral spectroscopy remains mostly unexplored in the current literature, despite the potential applications in the food industry and the biomedical sector. In this work, we have shown that the detailed interpretation of NIR signals is also possible with VCD, with higher sensitivity compared to standard absorption spectroscopy, on molecular systems of medium-size with several conformational degrees of freedom.

Dedication

We are glad to honor Professor Lawrence A. Nafie for his many contributions to VOA. We are also grateful for his friendship.

CRediT authorship contribution statement

Marco Fusè: Conceptualization, Investigation, Data acquisition and Data curation, Software, Methodology, Writing – original draft, Writing – review & editing. **Giuseppe Mazzeo:** Investigation, Data acquisition, Writing – review & editing. **Julien Bloino:** Software, Methodology, Writing – review & editing, Funding acquisition. **Giovanna Longhi:** Conceptualization, Methodology, Writing – original draft, Writing – review & editing, Funding acquisition. **Sergio Abbate:** Conceptualization, Methodology, Writing – original draft, Writing – review & editing, Funding acquisition.

Declaration of competing interest

The authors declare that they have no known competing financial interests or personal relationships that could have appeared to influence the work reported in this paper.

Data availability

Data will be made available on request.

Acknowledgments

The authors thank David A. Lightner of University of Nevada, Reno for helpful discussions, for encouraging VCD research in the NIR region and for providing us the 19-cm cuvette used for the VCD measurements in the 700–600 nm region.

Funding was provided by the Italian Ministry of University and Research (MUR) through the PRIN program (PRIN 2017, project "Physicochemical Heuristic Approaches: Nanoscale Theory of Molecular Spectroscopy" (PHANTOMS), prot. 2017A4XRCA and PRIN 2020, project "Photoreactive Systems upon Irradiation: Modelling and Observation of Vibrational Interactions with the Environment" (PSI-MOVIE), prot. 2020HTSXMA). The CINECA award under the ISCRA (IsC97_CSoVCS) initiative is acknowledged for providing high-performance computing facilities. Computing facilities from SNS HPC are also acknowledged.

Appendix A. Supplementary data

Supplementary material related to this article can be found online at https://doi.org/10.1016/j.saa.2023.123496. Additional experimental spectra; computed relative energy of the conformers; harmonic and IDVPT2 results; local-modes integrals and additional figures for local-mode analysis; molecular geometries in XYZ format.

References

[1] G. Herzberg, Molecular Spectra and molecular structure, Vol. II, D Van Nonstrad Company, Inc., 1945.
[2] E.B. Wilson, J.C. Decius, P.C. Cross, Molecular Vibrations: The Theory of Infrared and Raman Vibrational Spectra, McGraw-Hill Book Company Inc., 1955.
[3] C.L. Braun, S.N. Smirnov, Why is water blue? J. Chem. Educ. 70 (8) (1993) 612, http://dx.doi.org/10.1021/ed070p612.
[4] S. Zhang, S. Liu, L. Shen, S. Chen, L. He, A. Liu, Application of near-infrared spectroscopy for the nondestructive analysis of wheat flour: A review, Curr. Res. Food Sci. 5 (2022) 1305–1312, http://dx.doi.org/10.1016/j.crfs.2022.08.006.
[5] K.B. Beć, J. Grabska, C.W. Huck, Near-infrared spectroscopy in bio-applications, Molecules 25 (12) (2020) http://dx.doi.org/10.3390/molecules25122948.
[6] K.B. Beć, J. Grabska, C.W. Huck, Principles and applications of miniaturized near-infrared (NIR) spectrometers, Chem. – Eur. J. 27 (5) (2021) 1514–1532, http://dx.doi.org/10.1002/chem.202002838.
[7] C. Sándorfy, Hydrogen bonding: How much anharmonicity? J. Mol. Struct. 790 (1) (2006) 50–54, http://dx.doi.org/10.1016/j.molstruc.2005.07.036, Horizons in Hydrogen Bond Research 2005.
[8] L. Paoloni, G. Mazzeo, G. Longhi, S. Abbate, M. Fusè, J. Bloino, V. Barone, Toward fully unsupervised anharmonic computations complementing experiment for robust and reliable assignment and interpretation of IR and VCD spectra from mid-IR to NIR: The case of 2,3-Butanediol and *trans* -1,2-cyclohexanediol, J. Phys. Chem. A 124 (2020) 1011–1024, http://dx.doi.org/10.1021/acs.jpca.9b11025.
[9] M.A. Czarnecki, Near-infrared spectroscopic study of hydrogen bonding in chiral and racemic octan-2-ol, J. Phys. Chem. A 107 (12) (2003) 1941–1944, http://dx.doi.org/10.1021/jp0270102.
[10] J. Grabska, M. Ishigaki, K.B. Beć, M.J. Wójcik, Y. Ozaki, Correlations between structure and near-infrared spectra of saturated and unsaturated carboxylic acids. Insight from anharmonic density functional theory calculations, J. Phys. Chem. A 121 (18) (2017) 3437–3451, http://dx.doi.org/10.1021/acs.jpca.7b02053.

[11] V. Vaida, J.S. Daniel, H.G. Kjaergaard, L.M. Goss, A.F. Tuck, Atmospheric absorption of near infrared and visible solar radiation by the hydrogen bonded water dimer, Q. J. R. Meteorol. Soc. 127 (575) (2001) 1627–1643, http://dx.doi.org/10.1002/qj.49712757509.

[12] H.G. Kjaergaard, D.L. Howard, Overtone spectroscopy: A sensitive probe of hydrogen bonding, ChemInform 37 (42) (2006) http://dx.doi.org/10.1002/chin.200642277.

[13] S. Abbate, G. Longhi, L. Ricard, C. Bertucci, C. Rosini, P. Salvadori, A. Moscowitz, Vibrational circular dichroism as a criterion for local-mode versus normal-mode behavior. Near-infrared circular dichroism spectra of some monoterpenes, J. Am. Chem. Soc. 111 (3) (1989) 836–840, http://dx.doi.org/10.1021/ja00185a008.

[14] S. Abbate, G. Longhi, S. Boiadjiev, D. Lightner, C. Bertucci, P. Salvadori, et al., Analysis of vibrational circular dichroism data in the near infrared and visible range, Enantiomer 3 (1998) 337–347.

[15] T. Keiderling, P. Stephens, Vibrational circular dichroism of overtone and combination bands, Chem. Phys. Lett. 41 (1) (1976) 46–48, http://dx.doi.org/10.1016/0009-2614(76)85243-8.

[16] E. Castiglioni, F. Lebon, G. Longhi, S. Abbate, Vibrational circular dichroism in the near infrared: Instrumental developments and applications, Enantiomer 7 (4) (2002-07) 161–173, http://dx.doi.org/10.1080/10242430212877.

[17] F. Gangemi, R. Gangemi, G. Longhi, S. Abbate, Experimental and ab-initio calculated vcd spectra of the first OH-stretching overtone of (1R)-(-) and (1S)-(+)-endo-Borneol, Phys. Chem. Chem. Phys. 11 (2009) 2683–2689, http://dx.doi.org/10.1039/B818432A.

[18] S. Abbate, E. Castiglioni, F. Gangemi, R. Gangemi, G. Longhi, NIR-VCD, vibrational circular dichroism in the near-infrared: Experiments, theory and calculations, Chirality 21 (2009) E242–E252, http://dx.doi.org/10.1002/chir.20805.

[19] S. Abbate, G. Longhi, F. Gangemi, R. Gangemi, S. Superchi, A.M. Caporusso, R. Ruzziconi, Electrical and mechanical anharmonicities from NIR-VCD spectra of compounds exhibiting axial and planar chirality: The cases of (S)-2,3-pentadiene and methyl-d3 (R)- and (S)-[2.2]paracyclophane-4-carboxylate, Chirality 23 (9) (2011-10) 841–849, http://dx.doi.org/10.1002/chir.21013.

[20] C. Guo, R.D. Shah, R.K. Dukor, T.B. Freedman, X. Cao, L.A. Nafie, Fourier transform vibrational circular dichroism from 800 to 10,000cm^{-1}: Near-IR-VCD spectral standards for terpenes and related molecules, Vib. Spectrosc. 42 (2) (2006-11) 254–272, http://dx.doi.org/10.1016/j.vibspec.2006.05.013.

[21] L.A. Nafie, R.K. Dukor, J.-R. Roy, A. Rilling, X. Cao, H. Buijs, Observation of Fourier transform near-infrared vibrational circular dichroism to 6150 cm^{-1}, Appl. Spectrosc. 57 (10) (2003) 1245–1249, http://dx.doi.org/10.1366/000370203769699108.

[22] M. Fusè, G. Longhi, G. Mazzeo, S. Stranges, F. Leonelli, G. Aquila, E. Bodo, B. Brunetti, C. Bicchi, C. Cagliero, J. Bloino, S. Abbate, Anharmonic aspects in vibrational circular dichroism spectra from 900 to 9000 cm–1 for methyloxirane and methylthiirane, J. Phys. Chem. A 126 (38) (2022) 6719–6733, http://dx.doi.org/10.1021/acs.jpca.2c05332.

[23] S. Abbate, G. Longhi, J.W. Givens, S.E. Boiadjiev, D.A. Lightner, A. Moscowitz, Observation of vibrational circular dichroism for overtone transitions with commercially available CD spectrometers, Appl. Spectrosc. 50 (5) (1996) 642–643, http://dx.doi.org/10.1366/0003702963905934.

[24] W. Kuhn, Optical rotatory power, Annu. Rev. Phys. Chem. 9 (1) (1958) 417–438.

[25] J.R.A. Moreno, T.R. Huet, J.J.L. González, Conformational relaxation of S-(+)-carvone and R-(+)-limonene studied by microwave Fourier transform spectroscopy and quantum chemical calculations, Struct. Chem. 24 (2013) 1163–1170, http://dx.doi.org/10.1007/s11224-012-0142-8.

[26] F. Gangemi, R. Gangemi, G. Longhi, S. Abbate, Calculations of overtone NIR and NIR-VCD spectra in the local mode approximation: Camphor and camphorquinone, Vib. Spectrosc. 50 (2009) 257–267, http://dx.doi.org/10.1016/j.vibspec.2009.01.004.

[27] Q. Yang, M. Mendolicchio, V. Barone, J. Bloino, Accuracy and reliability in the simulation of vibrational spectra: A comprehensive benchmark of energies and intensities issuing from generalized vibrational perturbation theory to second order (GVPT2), Front. Astron. Space Sci. 8 (2021-05-31) 665232, http://dx.doi.org/10.3389/fspas.2021.665232.

[28] V. Barone, M. Biczysko, J. Bloino, Fully anharmonic IR and Raman spectra of medium-size molecular systems: accuracy and interpretation, Phys. Chem. Chem. Phys. 16 (5) (2014) 1759–1787, http://dx.doi.org/10.1039/C3CP53413H.

[29] S. Abbate, G. Longhi, E. Castiglioni, Near-infrared vibrational circular dichroism: NIR-VCD, in: Comprehensive Chiroptical Spectroscopy, John Wiley & Sons, Ltd, 2011, pp. 247–273, http://dx.doi.org/10.1002/9781118120187.ch10.

[30] M.J. Frisch, G.W. Trucks, H.B. Schlegel, G.E. Scuseria, M.A. Robb, J.R. Cheeseman, G. Scalmani, V. Barone, G.A. Petersson, H. Nakatsuji, X. Li, M. Caricato, A.V. Marenich, J. Bloino, B.G. Janesko, R. Gomperts, B. Mennucci, H.P. Hratchian, J.V. Ortiz, A.F. Izmaylov, J.L. Sonnenberg, D. Williams-Young, F. Ding, F. Lipparini, F. Egidi, J. Goings, B. Peng, A. Petrone, T. Henderson, D. Ranasinghe, V.G. Zakrzewski, J. Gao, N. Rega, G. Zheng, W. Liang, M. Hada, M. Ehara, K. Toyota, R. Fukuda, J. Hasegawa, M. Ishida, T. Nakajima, Y. Honda, O. Kitao, H. Nakai, T. Vreven, K. Throssell, J.A.M. Jr., J.E. Peralta, F. Ogliaro, M.J. Bearpark, J.J. Heyd, E.N. Brothers, K.N. Kudin, V.N. Staroverov, T.A. Keith, R. Kobayashi, J. Normand, K. Raghavachari, A.P. Rendell, J.C. Burant, S.S. Iyengar, J. Tomasi, M. Cossi, J.M. Millam, M. Klene, C. Adamo, R. Cammi, J.W. Ochterski, R.L. Martin, K. Morokuma, O. Farkas, J.B. Foresman, D.J. Fox, Gaussian16 Revision C.01, Gaussian Inc., Wallingford CT, 2016.

[31] A.D. Becke, Density-functional thermochemistry. III. The role of exact exchange, J. Chem. Phys. 98 (7) (1993-04) 5648–5652, http://dx.doi.org/10.1063/1.464913.

[32] E. Papajak, J. Zheng, X. Xu, H.R. Leverentz, D.G. Truhlar, Perspectives on basis sets beautiful: Seasonal plantings of diffuse basis functions, J. Chem. Theory Comput. 7 (10) (2011-10-11) 3027–3034, http://dx.doi.org/10.1021/ct200106a.

[33] M. Śmiałek, M.-J. Hubin-Franskin, J. Delwiche, D. Duflot, N.J. Mason, S. Vrønning-Hoffmann, G. De Souza, A.F. Rodrigues, F. Rodrigues, P. Limão-Vieira, Limonene: electronic state spectroscopy by high-resolution vacuum ultraviolet photoabsorption, electron scattering, He (I) photoelectron spectroscopy and ab initio calculations, Phys. Chem. Chem. Phys. 14 (6) (2012) 2056–2064, http://dx.doi.org/10.1039/C2CP22847E.

[34] M.M. Rafiee Fanood, H. Ganjitabar, G.A. Garcia, L. Nahon, S. Turchini, I. Powis, Intense vibronic modulation of the chiral photoelectron angular distribution generated by photoionization of limonene enantiomers with circularly polarized synchrotron radiation, ChemPhysChem 19 (8) (2018) 921–933, http://dx.doi.org/10.1002/cphc.201701248.

[35] J. Bloino, A VPT2 route to near-infrared spectroscopy: The role of mechanical and electrical anharmonicity, J. Phys. Chem. A 119 (21) (2015) 5269–5287, http://dx.doi.org/10.1021/jp509985u.

[36] M.J. Frisch, G.W. Trucks, H.B. Schlegel, G.E. Scuseria, M.A. Robb, J.R. Cheeseman, G. Scalmani, V. Barone, G.A. Petersson, H. Nakatsuji, X. Li, M. Caricato, A.V. Marenich, J. Bloino, B.G. Janesko, R. Gomperts, B. Mennucci, H.P. Hratchian, J.V. Ortiz, A.F. Izmaylov, J.L. Sonnenberg, D. Williams-Young, F. Ding, F. Lipparini, F. Egidi, J. Goings, B. Peng, A. Petrone, T. Henderson, D. Ranasinghe, V.G. Zakrzewski, J. Gao, N. Rega, G. Zheng, W. Liang, M. Hada, M. Ehara, K. Toyota, R. Fukuda, J. Hasegawa, M. Ishida, T. Nakajima, Y. Honda, O. Kitao, H. Nakai, T. Vreven, K. Throssell, J.A. Montgomery Jr., J.E. Peralta, F. Ogliaro, M.J. Bearpark, J.J. Heyd, E.N. Brothers, K.N. Kudin, V.N. Staroverov, T.A. Keith, R. Kobayashi, J. Normand, K. Raghavachari, A.P. Rendell, J.C. Burant, S.S. Iyengar, J. Tomasi, M. Cossi, J.M. Millam, M. Klene, C. Adamo, R. Cammi, J.W. Ochterski, R.L. Martin, K. Morokuma, O. Farkas, J.B. Foresman, D.J. Fox, Gaussian Development Version, Revision J.19, Gaussian, Inc., Wallingford CT, 2021.

[37] Q. Yang, J. Bloino, An effective and automated processing of resonances in vibrational perturbation theory applied to spectroscopy, J. Phys. Chem. A 126 (49) (2022) 9276–9302, http://dx.doi.org/10.1021/acs.jpca.2c06460.

[38] J.M.L. Martin, T.J. Lee, P.R. Taylor, J.-P. François, The anharmonic force field of ethylene, C2H4, by means of accurate ab initio calculations, J. Chem. Phys. 103 (7) (1995) 2589–2602, http://dx.doi.org/10.1063/1.469681.

[39] J. Bloino, ESTAMPES: A prototypical program for spectral analysis., 2020, GitHub repository, GitHub. https://github.com/jbloino/estampes (Accessed 24 August 2023).

[40] J.D. Hunter, Matplotlib: A 2D graphics environment, Comput. Sci. Eng. 9 (3) (2007) 90–95, http://dx.doi.org/10.1109/MCSE.2007.55.

[41] J.A.C. Gallas, Some matrix elements for morse oscillators, Phys. Rev. A 21 (6) (1980-06-01) 1829–1834, http://dx.doi.org/10.1103/PhysRevA.21.1829.

[42] A.B. McCoy, Curious properties of the Morse oscillator, Chem. Phys. Lett. 501 (4) (2011-01) 603–607, http://dx.doi.org/10.1016/j.cplett.2010.11.065.

[43] T.A. Keiderling, P. Bouř, Theory of molecular vibrational Zeeman effects as measured with circular dichroism, Phys. Rev. Lett. 121 (2018) 073201, http://dx.doi.org/10.1103/PhysRevLett.121.073201.

[44] M. Fusè, G. Mazzeo, G. Longhi, S. Abbate, lcmodslib: a small library for local mode approach, 2023, GitHub repository, GitHub. https://github.com/ledragna/lcmodslib. (Accessed 28 August 2023).

[45] K.V. Reddy, D.F. Heller, M.J. Berry, Highly vibrationally excited benzene: Overtone spectroscopy and intramolecular dynamics of C6H6, C6D6, and partially deuterated or substituted benzenes, J. Chem. Phys. 76 (6) (1982) 2814–2837, http://dx.doi.org/10.1063/1.443384.

[46] L. Laux, V. Pultz, S. Abbate, H.A. Havel, J. Overend, A. Moscowitz, D.A. Lightner, Inherently dissymmetric chromophores and vibrational circular dichroism. The CH2-CH2-C*H fragment, J. Am. Chem. Soc. 104 (15) (1982) 4276–4278, http://dx.doi.org/10.1021/ja00379a052.

[47] B.R. Henry, Use of local modes in the description of highly vibrationally excited molecules, Acc. Chem. Res. 10 (6) (1977-06-01) 207–213, http://dx.doi.org/10.1021/ar50114a003.

[48] D. McKean, Individual CH bond strengths in simple organic compounds: effects of conformation and substitution, Chem. Soc. Rev. 7 (3) (1978) 399–422, http://dx.doi.org/10.1039/CS9780700399.

[49] G. Longhi, L. Ricard, S. Abbate, G. Zerbi, A comparative study of the fundamental and overtone spectra of dioxane, J. Mol. Struct. 141 (1986) 325–330, http://dx.doi.org/10.1016/0022-2860(86)80343-X.

[50] G. Longhi, G. Zerbi, G. Paterlini, L. Ricard, S. Abbate, Conformational dependence of CH (CD)-strechings in D-glucose and some deuterated derivatives as revealed by infrared and raman spectroscopy, Carbohydr. Res. 161 (1) (1987) 1–22, http://dx.doi.org/10.1016/0008-6215(87)84001-6.

[51] E.D. Glendening, A.E. Reed, J.E. Carpenter, F. Weinhold, NBO Version 3.1.

[52] J.P. Foster, F. Weinhold, Natural hybrid orbitals, J. Am. Chem. Soc. 102 (24) (1980) 7211–7218, http://dx.doi.org/10.1021/ja00544a007.
[53] A.E. Reed, L.A. Curtiss, F. Weinhold, Intermolecular interactions from a natural bond orbital, donor-acceptor viewpoint, Chem. Rev. 88 (6) (1988) 899–926, http://dx.doi.org/10.1021/cr00088a005.
[54] L.A. Nafie, T.H. Walnut, Vibrational circular dichroism theory: a localized molecular orbital model, Chem. Phys. Lett. 49 (3) (1977) 441–446, http://dx.doi.org/10.1016/0009-2614(77)87010-3.
[55] L.A. Nafie, P.L. Polavarapu, Localized molecular orbital calculations of vibrational circular dichroism. I. General theoretical formalism and CNDO results for the carbon–deuterium stretching vibration in neopentyl-1-d-chloride, J. Chem. Phys. 75 (6) (1981) 2935–2944, http://dx.doi.org/10.1063/1.442384.
[56] H. Takahashi, K. Takahashi, S. Yabushita, Interpretation of semiclassical transition moments through wave function expansion of dipole moment functions with applications to the OH stretching spectra of simple acids and alcohols, J. Phys. Chem. A 119 (20) (2015) 4834–4845, http://dx.doi.org/10.1021/acs.jpca.5b02050.
[57] M. Tsuyuki, S. Furudate, Y. Kugaya, S. Yabushita, Graphical transition moment decomposition and conceptual density functional theory approaches to study the fundamental and lower-level overtone absorption intensities of some OH stretching vibrations, J. Phys. Chem. A 125 (10) (2021) 2101–2113, http://dx.doi.org/10.1021/acs.jpca.0c11619.
[58] G. Longhi, S. Abbate, C. Zagano, G. Botto, L. Ricard-Lespade, Analysis of the transition from normal modes to local modes in a system of two harmonically coupled morse oscillators, Theor. Chim. Acta 82 (3) (1992) 321–337, http://dx.doi.org/10.1007/BF01113262.